# An enhanced statistical shape model for automatic feature segmentation of human vertebrae

Antonio Marzola [a],[*], Luca Di Angelo [b], Paolo Di Stefano [b], Yary Volpe [a]

[a] *Department of Industrial Engineering, University of Florence, 50139, Firenze, Italy*
[b] *Department of Industrial and Information Engineering and Economics, University of L'Aquila, 67040, L'Aquila, Italy*

## ARTICLE INFO

## ABSTRACT

*Background & objective:* Human vertebrae are analysed and measured for various purposes, including to study anatomy, to diagnose illness, and to evaluate therapies. Achieving an accurate morphological and dimensional characterisation of three-dimensional (3D) vertebrae relies on the precise recognition of their features. Traditionally, these features, lacking defined edges, have been identified manually through a time-consuming, poorly repeatable, and poorly reproducible process. To the authors' knowledge, there is only one method published in the literature able to automatically recognise all the most important vertebral features: the algorithmic feature recognition method (AFRM). It requires a high-density point cloud as input, the presence of all morphological features, even if incomplete, and incurs high computational costs. This research aims to propose an improved version of the AFRM to overcome its limitations.
*Methods:* The proposed approach combines the robustness of AFRM to provide the semantic segmentation of a 3D healthy human vertebra with the ability of the enhanced statistical shape model (eSSM) to transfer information among different models. Specifically, AFRM provides the semantic segmentation of the mean shape of the eSSM, while the latter transfers this information to target shapes.
*Results:* The eSSM was developed using 20 training samples of healthy adult male L2 vertebrae. The test samples included five healthy vertebrae and four vertebras with large missing parts. None of the test shapes were included in the training set. The novel approach could accurately recognise morphological features without the constraints that affect the AFRM.
*Conclusion:* The proposed method guarantees reliable and automated segmentation through AFRM, exploiting the eSSM's ability to provide results even when dealing with sparsely populated or partially incomplete target models, significantly reducing the computational load.

## 1. Introduction

The human vertebrae are morphologically complex bones that protect the spinal cord, house nerves and muscle roots, and support the body. Due to the spatial distribution of their morphologic features (including the vertebral body, vertebral foramen, the superior and inferior articular processes, the spinous process, the transverse processes, and the lamina), information about the functionality and deformities of vertebrae must be obtained by analysing the correlation between three-dimensional (3D) characteristics. For this reason, numerous methods analysing the relationship between 3D features and common pathologies, considering both the entire spinal column and individual vertebrae, have been proposed in the related literature.

Among the methods that analyse the whole spine, those of interest are:

- Steib et al. [1] examined the vertebral axial rotation and the torsion of patients with scoliosis before and after surgery.
- Nault et al. [2] investigated the Cobb angles, the plane of maximal deformation, 3D wedging of the vertebral body and disk, axial intervertebral rotation, torsion, and slenderness to predict the progression of adolescent idiopathic scoliosis.
- Ferrero et al. [3] analysed relationships among rotatory subluxation in adult spinal deformity, transverse plane parameters, spinopelvic parameters, and clinical outcomes.

* Corresponding author.
  *E-mail address:* antonio.marzola@unifi.it (A. Marzola).

- Wu and Wong [4] proposed that the most significant descriptors used to describe the 3D features of scoliosis are the plane of maximum curvature, end-apical-end vertebrae, and the best-fit plane.

Regarding 3D analysis of the individual vertebra, the following publications can be considered relevant:

- Wang et al. [5] and Kishimoto et al. [6] proposed the estimation of stress and pressure in intervertebral discs, valuing disc volume, and sizing spinal implants by measuring the endplates' surface area.
- Otsuka et al. [7] presented a study relating loading and stress transfer on spinal implants to the lumbar facet joint area and orientation.
- Simon et al. [8] proposed a correlation between osteoarthritis and the facets' joint space.

The main limitation of the above methods is that they require a skilled operator who manually segments the morphological features and measures the required dimensional parameters. This process is tedious and time-consuming, and the result depends on the preparation and the operator's knowledge, thus producing poorly objective assessments. Consequently, these manual quantitative evaluations must often be analysed by considering bias due to their intrinsic poor repeatability and reproducibility.

To overcome these limitations, in 2021 Di Angelo et al. [9] proposed, to the best of the authors' knowledge, the first and still the only automated methodology for segmenting and recognising the most important morphological features of 3D human thoracic and lumbar vertebrae. The method requires only the 3D discrete model of the vertebra as input, extrapolated from diagnostic imaging and provided in the STL or OBJ format. No further interaction is required from the user. Based on semantic and geometric segmentation, the algorithm proposed by Di Angelo et al. [9] – called the algorithmic feature recognition method (AFRM) in this paper – uses rules customised to the thoracic and lumbar vertebral morphology information that is invariant among subjects. Di Angelo et al. [9] demonstrated the robustness and reliability of this method. Compared with the state-of-the-art methods for the manual segmentation and measurement of 3D human vertebrae, the AFRM represents a considerable improvement in evaluating the 3D parameters of morphological features. On the other hand, to ensure consistent results, the AFRM requires a high-density point cloud as an input (almost 0.5 mm) and the presence, even if incomplete, of all the morphological features. These constraints are mainly because the algorithm associates the points of the model with specific morphological features and then approximates them by using characteristic analytical surfaces. This processing, which requires substantial computational time, is based on analysing the differential discrete properties of models with a globally symmetrical structure.

Because the aforementioned shortcomings can be restrictive when studying large quantities of vertebrae, especially pathological ones, this paper proposes a new methodology based on integration of the AFRM with the enhanced statistical shape model (eSSM) [10]. The eSSM is an improvement of the traditional statistical shape model (SSM), a population-based model able to encode in a convenient mathematical framework the geometric characteristics and patterns observed at the population level. The individuals that comprise the population used in the analysis possess shared attributes that enable their categorisation as belonging to a specific family of shapes (e.g., human lumbar vertebrae). The SSM is particularly valuable for studying complex shapes where individual heterogeneity plays a crucial role in shaping the distinctive characteristics of the population. Compared with the traditional SSM, the eSSM enables the collection of additional information beyond geometric data. In the methodology proposed in this paper, the additional information collected by the eSSM includes the semantic segmentation obtained through the AFRM: the idea is to combine the robustness of the AFRM to provide the semantic segmentation of a reference model with the eSSM's ability to transfer information across models. Specifically, the AFRM provides the semantic segmentation of the mean shape of the eSSM, while the eSSM transfers this information to target shapes.

The proposed methodology has been applied to adult male L2 vertebrae. After constructing the eSSM with 20 healthy training samples, the procedure's performance was verified by analysing healthy L2 vertebrae not included in the training set (TS) and vertebrae that were appropriately modified by erasing morphological features totally or partially. The proposed procedure permitted the automatic extraction and segmentation of morphological features with a low computational cost and robust results, even for models with low resolution or significant missing areas. The findings indicate that the proposed methodology, which includes integration of the eSSM, maintains the same robustness as the AFRM, even for models with low resolution and/or a complete lack of morphological features.

## 2. Automatic 3D feature segmentation methods of human thoracic and lumbar vertebrae

The term 'segmentation' in the biomedical field is usually used to identify the process of constructing a 3D geometric model from a collection of two-dimensional (2D) images [10]. To generate tools for vertebral segmentation from computed tomography (CT) and magnetic resonance imaging (MRI) scans, many of the latest published methods use approaches based on convolutional neural networks [11–13] or deep learning [14]. Instead, in this research, segmentation refers to grouping the triangular mesh nodes in features according to their surface properties. For vertebrae, this segmentation process is an essential preliminary step in determining the dimensional features of the spinal column or individual vertebrae, especially those related to common pathologies. Despite its importance, segmentation is usually still performed manually due to the lack of available tools capable of automatically segmenting and recognising the morphological features of 3D models of human vertebrae. The reason for this is that the segmentation process is very complex to perform algorithmically, as it requires recognising high-level data from low-level geometric information. Specifically, when working on a discrete model, only the vertex coordinates of the geometric grid representing the external surface of the 3D model are known. To the authors' knowledge, there are only two papers that have published methods for the automatic segmentation of the morphological features of a human vertebra [9,15].

Cheng et al. [15] proposed a topological data analysis–based method to segment and recognise the morphological features of the 3D vertebra. In particular, the Reeb graph [16] is adopted for topological data analysis, and a cycle-detect-based algorithm is used to separate the morphological features of the 3D vertebra. The main limitation of this method is neglecting important morphological features such as superior and inferior articular processes. This limitation has been overcome by the method proposed by Di Angelo et al. [9] (the aforementioned AFRM). Those authors demonstrated that the AFRM can segment all the most important morphological and geometric features of thoracic and cervical vertebrae.

The AFRM is based on the following three steps:

- Local coordinate system (LCS) identification (Fig. 1a);
- 3D morphological feature recognition (Fig. 1c); and
- 3D geometric features segmentation and approximation (Table 1).

First, the LCS is identified according to Klinder et al. [17] (Fig. 1a):

- The origin is located where the middle plane intersects the axis of the largest cylinder contained in the vertebral foramen.
- The z-axis is perpendicular to the middle plane.
- The x-axis belongs to the symmetry plane and is orthogonal to the z-axis.
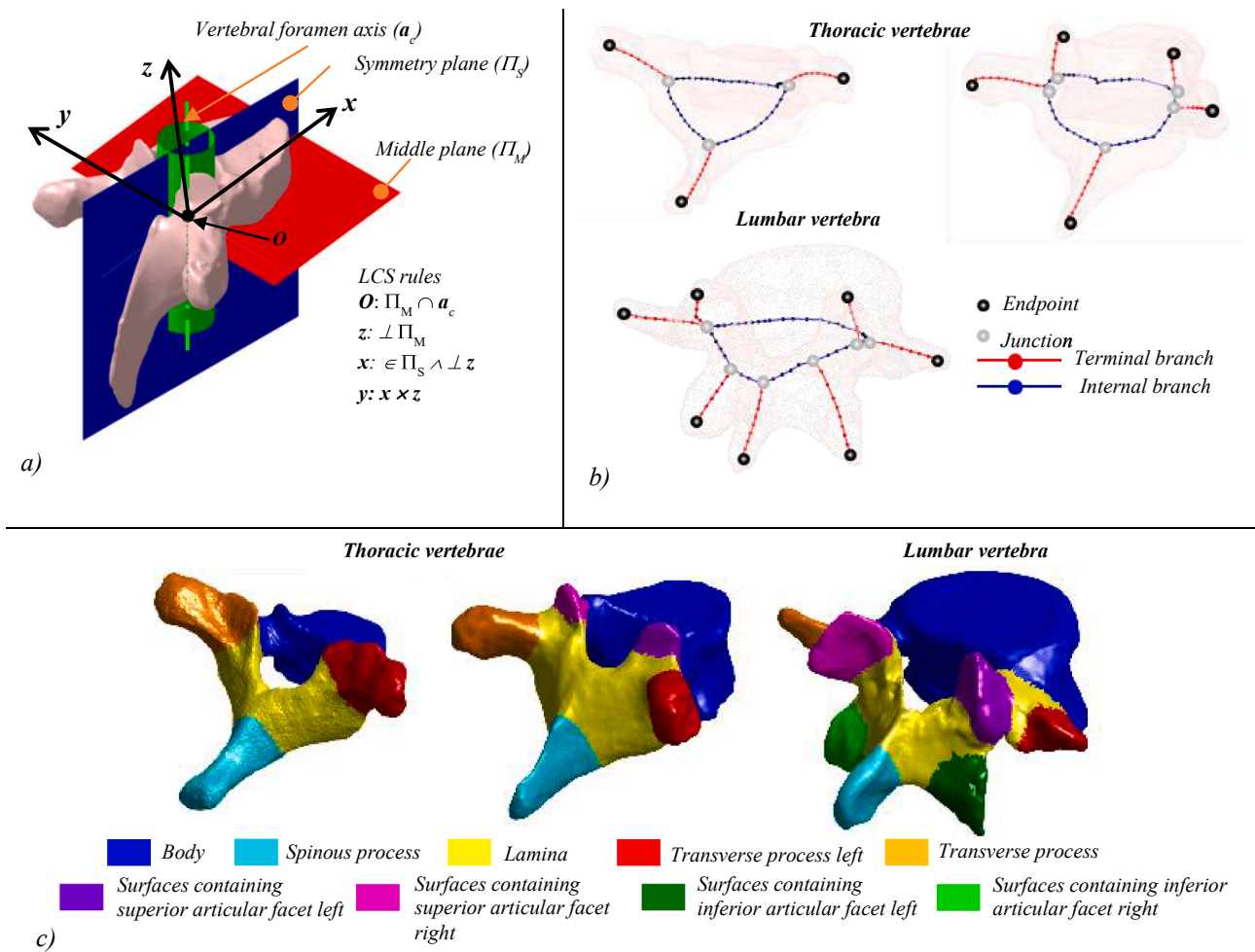- The y-axis is perpendicular to the x-axis and z-axis.

**Fig. 1.** The key steps of the automatic human vertebral morphological segmentation method.

Di Angelo et al. [9] describe the procedures utilised to identify all the derived geometric features for evaluating LCS.

Following the alignment of the vertebra to the LCS, the method calculates a descriptor derived from its geometric model known as the skeleton line – a curve inside the object, farthest from the external surface [18]. The skeleton line is a graph $\mathscr{G} = (\mathscr{N}, \mathscr{B})$ consisting of nodes ($\mathscr{N}$) connected by branches ($\mathscr{B}$). A node is defined as follows based on the number of connected branches:

- A *junction-node* ($N_h^J$) if at least three branches start from it;
- An *internal-node* ($N_k^I$) if two branches pass from it;
- An *end-node* ($N_l^E$) if it is connected to only one branch.

Consequently, the branches are labelled as *terminal* ($B_m^T$) or *internal* ($B_n^I$) depending on whether they are bounded by an *end-node* (Fig. 1b). By analysing the 3D position and spatial distribution of the three types of nodes and the two types of branches of the skeleton line, the following specific rules are defined to recognise the considered morphological features (Fig. 1c):

- The *right* (left) *transverse process* consists of the points collapsing into *terminal branches*, whose *end-node* has the maximum (minimum) y coordinate of the skeleton line points.
- The *spinous process* consists of the points collapsing into *terminal branches*, whose *end-node* has the maximum x coordinate of the skeleton line points.

- The *body* consists of points collapsed into the *internal branch* with the minimum x coordinate of the skeleton line points.
- The inferior (superior) articular processes (whose number depends on the vertebral morphology) are associated with those points collapsed into the couples of terminal branches, which are located quite symmetrically to the sagittal plane and whose orientation is mainly downward (upward) along the z-axis.
- The *lamina* corresponds to the points of the two remaining internal branches, located roughly symmetrically to the sagittal plane.
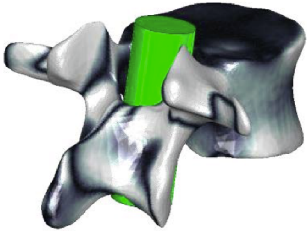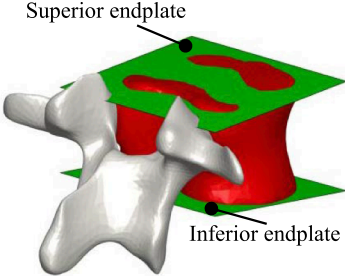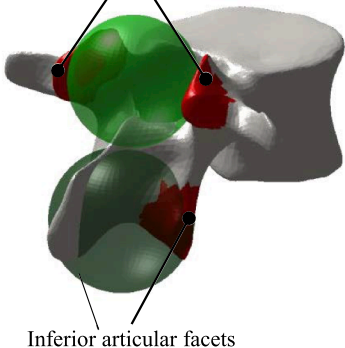
Original strategies are implemented to prune the skeleton line of terminal branches not clustered according to the previous definition for vertebrae with particular morphology and/or pathologies. Furthermore, based on dihedral angle analysis, a specific region-growing algorithm is introduced to associate the junction points with suitable semantic features.

The third step of the methodology aims to identify and estimate the 3D geometric features of the recognised lumbar and thoracic vertebral morphological features. Table 1 reports, for each of the considered morphological features, the corresponding identification rules, approximating the surfaces used, and the dimensional features evaluated. More details of the methodology can be found in the publication by Di Angelo et al. [9].

Di Angelo et al. [9] demonstrated the method's potential to automatically obtain robust and reliable segmentation and recognition of human thoracic and lumbar vertebral morphological features. However, because the method based on morphological analysis begins with a discrete vertebral model, it requires:

**Table 1**

The recognised morphological features, the corresponding rules, approximating the surfaces used, and the dimensional features evaluated by Di Angelo et al. [9].

| Morphological feature | Identification rules | Approximating surface | Dimensional features | Example |
|---|---|---|---|---|
| *Vertebral foramen* | Concave area enclosed between the body and the lamina | Largest diameter insertable into the vertebral foramen | The radius ($r_{vf}$) and angle ($\alpha_{vf}$) between the axis of the cylinder and the z-axis of each LCS | |
| The *superior endplates* on the body | Adjacent triangles positioned above the barycentre of the body for which the dot product of their normal versors and the normal versor of the middle plane is greater than 0 | Plane ($\Pi_S$) | Surface area ($A_{es}$) and projected surface area ($A_{es}^p$) on $\Pi_S$ of the superior endplate | |
| The *inferior endplates* on the body | Adjacent triangles positioned below the barycentre of the body for which the dot product of their normal versors and the normal versor of the middle plane is lower than 0 | Plane ($\Pi_I$) | Surface area ($A_{is}$) and projected surface area ($A_{is}^p$) on $\Pi_i$ of the superior endplate | |
| The *superior articular facet* | • Located on surfaces containing superior articular facets (if segmented); Symmetrically arranged with respect to the sagittal plane; Face directly posteriorly or posteromedially. | Sphere ($s_{saf}$) | Coordinates of the centres ($[x_{saf}, y_{saf}, $ and $z_{saf}]$ and radii ($r_{saf}$) of $s_{af}$ | |
| The *inferior articular facet* | • Located on surfaces containing inferior articular facets (if segmented); Symmetrically arranged with respect to the sagittal plane; Face directly anteriorly or anterolaterally. | Sphere ($s_{iaf}$) | Coordinates of the centres ($[x_{iaf}, y_{iaf}, $ and $z_{iaf}]$), and radii ($r_{iaf}$) of $s_{af}$ | |

- A discrete vertebral model with a sufficiently high density for the segmentation and recognition of morphological and dimensional properties.
- The presence of all morphological features on the vertebra, even if incomplete.
- A long calculation time for the skeleton line evaluation.

These limits are restrictive when analysing large quantities of vertebrae, especially pathological samples.

## 3. The proposed methodology

The methodology presented by Di Angelo et al. [9] is based on the codification of experienced operators' knowledge of segment morphological features of the thoracic and lumbar vertebrae into rules. This approach results in a robust and coherent outcome, but it is also affected by the limitations discussed above. This paper proposes a more efficient methodology that exploits the ability of the eSSM to interpret the rules encoded in the AFRM to segment a new target shape.

There are several reasons for choosing a statistical shape analysis (SSA)-based method over predictive methods:

- The data have specific shape-based characteristics that align well with the strengths of SSA [19];
- The limitations imposed by the dataset's constraints: there is limited availability of CT scans of healthy vertebrae for training the model;
- The incoherence between the TS (healthy vertebrae) and potential targets (partially missed vertebrae): one of the objectives of the proposed method is to ensure reliable and coherent segmentation even in cases involving 3D models with large missing parts (i.e., very different from those included in the TS).

For all these reasons, to the best of the authors' knowledge, methods based on artificial intelligence, such as machine learning techniques, have not been applied in published approaches for the semantic segmentation of anatomical features of the 3D model of a human vertebra.

In recent decades, SSA has proved to be one of the most potent tools for quantitatively analysing anatomical shapes [20]. In the typical approach, SSA employs multivariate statistical methods to infer common patterns in shape variations of an anatomical structure from an initial set of training data (the TS) that reproduce the same structure. The inferred information is then encoded in a mathematically sound framework able to reproduce coherent shapes similar to those contained in the TS by applying well-defined and bounded deformation on a reference shape called the mean shape. The result is the parametric SSM. When the models forming the TS are provided as point distribution models (PDM), the SSM has the following form:

$$\mathbf{x} = \bar{\mathbf{x}} + \sum_{m=1}^{c} \alpha_m \sqrt{\lambda_m} \phi_m, \tag{1}$$

where:

- $\bar{\mathbf{x}}$ Is the mean shape
- $\sqrt{\lambda_m}$ are the magnitudes of the allowed deformations;
- $\phi_m$ are the directions of the allowed deformations;
- $\sqrt{\lambda_m} \phi_m$ with $m = 1, ..., c$ are known as the modes of variations (MoVs);
- $c$ represents the number of MoVs assessed to compute the SSM;
- $\alpha = [\alpha_1, \alpha_2, \cdots, \alpha_c]$ is a coefficient vector that extends the deformation allowed by the MoVs.

The magnitudes $\sqrt{\lambda_m}$ and directions $\phi_m$ are defined by applying principal component analysis (PCA) to the initial TS. A higher value of $c$ implies considering more variation described by the TS, but it comes at the expense of an increased computational burden. The highest value of $c$ is determined as the minimum between the number of training samples and the number of points in each PDM.

Each component of $\alpha$ is limited to the range $[-3; +3]$ to avoid implausible shapes, corresponding to a deformation that is three standard deviations away from the mean. When $\alpha = 0$, the resulting model $\mathbf{x}$ equals the mean shape. By varying the vector $\alpha$, Eq. (1) produces a new shape $\mathbf{x}$ that belongs to the same family of shapes as those contained in the TS. For a comprehensive description of the SSA procedure and its mathematical framework, see Marzola et al. [21].

Among the many applications of SSA in biology, the most interesting ones for the application discussed in this paper are related to the medical field. SSA has been applied, for example, for the automatic segmentation of diagnostic images [20], such as CT and MRI, or to infer the most likely healthy shape for deformed or partially missing anatomical regions, leveraging known regions as prior knowledge [21]. SSA could also be employed to generate new coherent shapes for testing purposes.

To increase the scope and capabilities of traditional SSA, Marzola et al. [22] proposed the eSSM: while the SSM can consider only geometric information, the eSSM enables the storage of additional functional points (e.g., centres of rotation, vertices of anatomical and mechanical axis, the position of the centre of gravity, etc.) and additional information on each point (e.g., semantic segmentation, location

of tendons and ligaments insertions, force application points, material, chemical or physical characteristics, etc.). Similarly to the traditional SSM, the eSSM can be used to match a target shape (whether whole or with missing parts) to transfer to the latter all the information encoded in the parametric model. This operation, called *fitting*, enriches the target shape with geometric (e.g., to retrieve the most likely shape for a missing region), functional (e.g., to provide the centres of rotation of a joint automatically), or descriptive (e.g., additional information on a point) information. Eq. (1) is still valid for the eSSM, which maintains the same mathematical framework and robustness as the traditional SSM, but it allows the user to tailor the information to be encoded and, if needed, to be transferred to the target model through the fitting operation.

The additional information to be considered depends on the application's specific requirements. For example, Marzola et al. [22] constructed an eSSM of the pelvis as a geometric reference to design prostheses for total hip replacements. This model was enriched with the positions of the hip joint's centres of rotation, critical information for ensuring proper prosthesis functionality.

Compared with the traditional SSM, the eSSM is more time-consuming and demands increased user interaction in setting up SSA. This increased time commitment is because the eSSM requires adding extra information either to each training shape (if there are additional points) or directly to the mean shape (if the information is defined on the points). On the other hand, the eSSM provides a much more comprehensive model that is able to supply valuable additional data, and thus saves time in the subsequent phases.

The differences between the mean shape resulting from the SSM and the eSSM are shown in Fig. 2. The enhanced mean shape (Fig. 2b) encloses the same information as the traditional mean shape regarding the external shape (Fig. 2a); in addition, it includes additional rows (in red) and columns (in blue). The additional rows can be used to store the spatial coordinates of other significant landmarks, and the additional columns define more information on each point than those related to their spatial position. In particular, in Fig. 2b:

- The red rows contain meaningful point coordinates added to the mean shape. These points must be selected before performing the SSA algorithm on all the training samples.
- The blue columns are incorporated into the mean shape to include information associated with each point, such as labels, weights, and other parameters. This information can be added after defining the SSM directly onto the mean shape, rather than applying it individually to all of the training samples. This approach is used because such information pertains to all corresponding points across all the training samples.

### 3.1. Construction and application of an eSSM for the semantic segmentation of a human vertebra

The eSSM proposed in this paper aims to construct a parametric and generative atlas of thoracic or lumbar human vertebrae with additional semantic segmentation information. Fig. 3 shows the workflow for constructing and applying the proposed eSSM.

The process starts by opportunely selecting a TS, which must include examples of the objects to be modelled without redundant and conflicting information. The MoVs and mean shape are obtained by applying the traditional SSA on the TS, without adding extra points to the training samples.

The segmented mean shape is then derived by applying the AFRM to the mean shape resulting from SSA. As a consequence, it has an additional column and no additional rows compared with the traditional SSM. Practically speaking, the segmentation is encoded in the data matrix of the mean shape by a specific label (a number from 1 to 9, Table 2) located in the fourth column in the same row of the point at
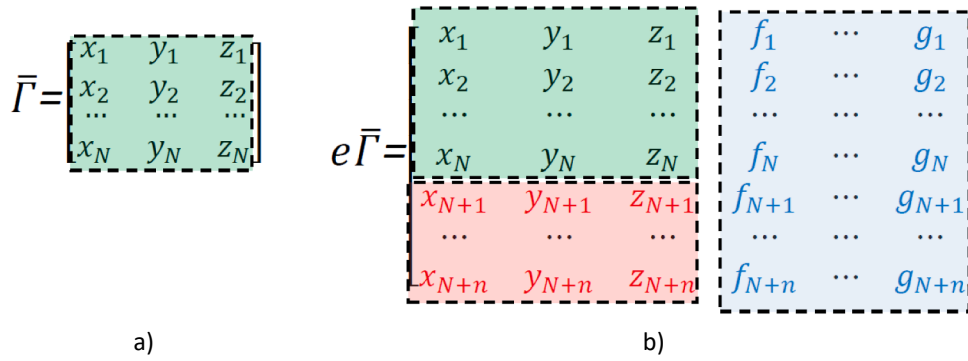
$$\bar{\Gamma} = \begin{bmatrix} x_1 & y_1 & z_1 \\ x_2 & y_2 & z_2 \\ ... & ... & ... \\ x_N & y_N & z_N \end{bmatrix}$$

$$e\bar{\Gamma} = \begin{bmatrix} x_1 & y_1 & z_1 & f_1 & \cdots & g_1 \\ x_2 & y_2 & z_2 & f_2 & \cdots & g_2 \\ ... & ... & ... & ... & \cdots & ... \\ x_N & y_N & z_N & f_N & \cdots & g_N \\ x_{N+1} & y_{N+1} & z_{N+1} & f_{N+1} & \cdots & g_{N+1} \\ ... & ... & ... & ... & \cdots & ... \\ x_{N+n} & y_{N+n} & z_{N+n} & f_{N+n} & \cdots & g_{N+n} \end{bmatrix}$$

a)                                          b)

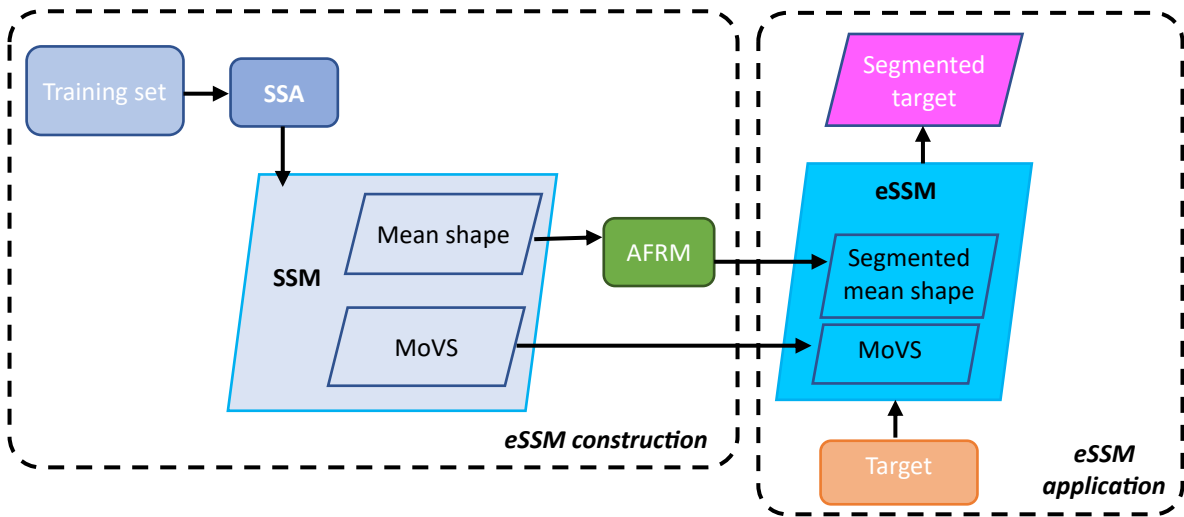**Fig. 2.** The mean shape for (a) the SSM and (b) the eSSM.



**Fig. 3.** The workflow for the construction and application of the eSSM encoding the semantic segmentation of the anatomical features of a thoracic or lumbar vertebra.

**Table 2**
Labels used in the eSSM to encode the segmentation in the mean shape data matrix.

| Label | Semantic feature |
|---|---|
| 1 | Body |
| 2 | Spinous process |
| 3 | Transverse process right |
| 4 | Transverse process left |
| 5 | Articular facet superior right |
| 6 | Articular facet superior left |
| 7 | Lamina |
| 8 | Articular facet inferior right |
| 9 | Articular facet inferior left |

$$e\bar{\Gamma} = \begin{bmatrix} x_1 & y_1 & z_1 & 1 \\ x_2 & y_2 & z_2 & 5 \\ ... & ... & ... & ... \\ x_i & y_i & x_i & 3 \\ ... & ... & ... & ... \\ x_j & y_j & z_j & 3 \\ ... & ... & ... & ... \\ x_k & y_k & z_k & 9 \\ ... & ... & ... & ... \\ x_h & y_h & z_h & 8 \\ ... & ... & ... & ... \\ x_m & x_m & x_m & 8 \\ ... & ... & ... & ... \\ x_N & y_N & z_N & 1 \end{bmatrix}$$

**Fig. 4.** An example of the mean shape matrix for the eSSM of a vertebra, where the fourth column defines the semantic segmentation of each row – that is, each point – through the nine different labels.

which the label is referred (Fig. 4). The result is that the segmented mean shape encodes information regarding both the location of each point and its segmentation. Finally, the eSSM is formed by using the same MoVs calculated from the traditional SSA and the segmented mean shape.

When a new vertebra (i.e., one that does not belong to the TS) is used as a target shape, the eSSM fits it using only the first three columns, following a process similar to traditional SSA. Each point on the mean shape is deformed during the fitting process to align with its corresponding point on the target model. As a consequence, the attribution of each point to its corresponding semantic feature in the target shape is automatically determined based on the related label in the fourth column without requiring any modifications or user interactions. These operations have a very low computational cost, as it requires only the
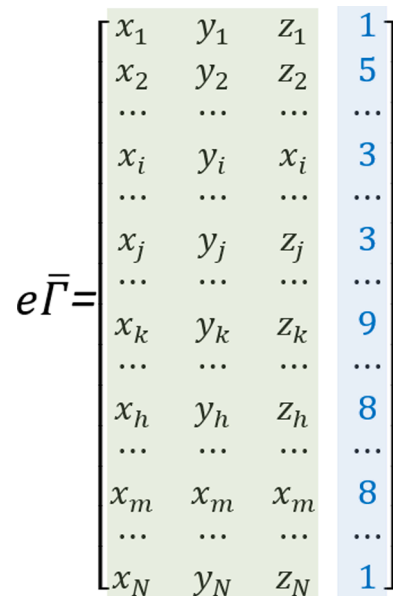
process of fitting the mean to the target model. Furthermore, the ability of the eSSM to infer the most likely shape from partial data can now be exploited to automatically analyse the 3D anatomical features even for models with large missing areas.

## 4. Results

This paper presents a test case involving L2 human vertebrae. The aim was to assess the effectiveness of the proposed approach in creating a parametric and generative atlas that automatically segments a target shape, even when a large area is missing from the target shape. The L2 vertebra was chosen for evaluation due to its significance in spinal functionality [23–25], but such a choice does not affect the conclusions of this paper, which can be generalised to other anatomies.

### 4.1. eSSM construction

A preliminary fundamental step to assess the methodology's performance was the collection of as many healthy L2 as possible to create the TS. Unfortunately, this step faced a significant challenge due to the limited availability of CT scans of healthy vertebrae. This problem is not specifically related to L2, but rather to all healthy vertebrae. As the number of training tests decreases, the eSSM's capacity to capture significant variability will be reduced.

The initial dataset consisted of 25 pathologically unaffected L2 vertebrae segmented from anonymised CT images collected from the online repository Spineweb [20–22]. T3DDY Lab [23] personnel conducted the segmentation process using Materialise Mimics 25®. This resulted in manifold tessellated models of the 25 L2 vertebrae with an average sample rate of 1.25 mm. Among these models, 20 were utilised as training samples to train the eSSM, while the remaining models were used for testing the results.

Due to its importance in the final result, investigations were carried out to assess the consistency of the TS. This step is fundamental to ensure that the TS is sufficiently uniform, as all the models involved in this study were obtained from an online repository of anonymised CT data. These investigations involved the segmentation, recognition, and calculation of the dimensional features of the 20 training samples using the AFRM, following the procedure described in Section 2. The purpose was to ensure no inconsistencies in shape or dimensions among the TS, which could result from segmentation errors or unidentified malformations. The results, reported in Table 3, confirmed that the training shapes exhibit significant variability but remain within the bounds of normal interpersonal variability observed in healthy vertebrae. Table 3, in addition to the dimensional features detailed in Table 1, shows two additional dimensional features related to the whole vertebra, namely the volume and the mean asymmetry calculated with respect to the symmetry plane $\Pi_s$ (Fig. 1a).

Subsequently, SSA was performed to infer the mean shape and the MoVs of the 20 training samples. The resulting SSM was evaluated based on the three characteristics proposed by Davies [26]:

- Generalisation (G),
- Specificity (S),
- Compactness (C).

These three characteristics were computed as described by Marzola et al. [21]. The results are presented in Figs. 5, 6, and 7, respectively.

G measures the model's ability to learn the characteristics of the family of shapes under consideration from a limited TS. It is estimated by performing a series of leave-one-out tests on the TS, measuring the distance of the omitted training shape to its closest match provided by the reduced SSM. As explained by Marzola et al. [21], G can be seen as an estimation of the statistical model's expected fitting error (in mm) under consideration. In this application, the fitting error remains relatively high (1.50 mm) with a significantly high standard deviation,

**Table 3**

The dimensional features of the 20 vertebrae used as the TS – segmented, recognised, and dimensioned according to Di Angelo et al. [9].

| Label | Whole vertebra | | Vertebral foramen | | Vertebral body | | | | | Superior articular facet | | | | Inferior articular facet | | | |
|---|---|---|---|---|---|---|---|---|---|---|---|---|---|---|---|---|---|
| | Volume [mm³] | Mean Asymmetry [mm] | $r_{vf}$ [mm] | $\alpha_{vf}$ [°] | $A_{es}$ [mm²] | $A_{es}^{p}$ [mm²] | $A_{is}$ [mm²] | $A_{is}^{p}$ [mm²] | $\alpha_{b}$ [°] | $x_{saf}$ [mm] | $y_{saf}$ [mm] | $z_{saf}$ [mm] | $r_{saf}$ [mm] | $x_{iaf}$ [mm] | $y_{iaf}$ [mm] | $z_{iaf}$ [mm] | $r_{iaf}$ [mm] |
| L2_1 | 44379.67 | 1.95 | 8.06 | 2.43 | 1132.2 | 1122.0 | 1291.6 | 1272.8 | 6.62 | 15.63 | 2.10 | 6.34 | 14.50 | 18.00 | 2.30 | −24.07 | 15.92 |
| L2_2 | 42836.34 | 0.84 | 7.39 | 1.81 | 1069.8 | 1050.3 | 1191.2 | 1161.5 | 7.63 | 18.27 | −0.75 | 8.36 | 15.48 | 18.01 | −0.27 | −21.86 | 15.90 |
| L2_3 | 26309.93 | 1.20 | 5.27 | 1.02 | 822.9 | 813.7 | 985.1 | 961.1 | 7.62 | 15.65 | −1.35 | 11.10 | 14.60 | 13.83 | 0.87 | −19.53 | 14.09 |
| L2_4 | 59015.21 | 1.38 | 5.99 | 3.49 | 1106.2 | 1088.6 | 1259.6 | 1238.4 | 3.10 | 21.78 | 0.37 | 6.51 | 19.59 | 25.60 | 1.32 | −21.20 | 24.87 |
| L2_5 | 45182.70 | 2.11 | 7.17 | −0.42 | 915.6 | 890.1 | 1066.0 | 1039.1 | 2.11 | 20.23 | 2.06 | 14.37 | 15.94 | 19.63 | −2.02 | −23.28 | 16.26 |
| L2_6 | 46139.18 | 4.28 | 7.92 | −3.61 | 1070.9 | 1051.0 | 1131.0 | 1111.7 | 2.50 | 15.65 | −4.48 | 19.48 | 14.79 | 14.47 | −1.65 | −20.10 | 14.24 |
| L2_7 | 63353.57 | 1.64 | 6.95 | 0.79 | 1500.0 | 1474.0 | 1603.1 | 1571.1 | 5.17 | 19.90 | 1.19 | 19.68 | 17.65 | 20.13 | 0.76 | −17.11 | 18.17 |
| L2_8 | 49384.23 | 1.16 | 7.61 | 1.84 | 1216.6 | 1189.8 | 1289.9 | 1270.1 | 2.21 | 16.57 | −0.53 | 11.38 | 15.46 | 17.59 | 0.91 | −23.89 | 16.21 |
| L2_9 | 58818.42 | 2.49 | 6.14 | −2.96 | 1202.5 | 1181.8 | 1392.9 | 1366.2 | 1.32 | 18.95 | 1.49 | 18.59 | 15.22 | 15.10 | 1.96 | −17.77 | 13.36 |
| L2_10 | 68294.61 | 0.99 | 7.96 | −4.45 | 1294.5 | 1250.7 | 1448.5 | 1404.7 | 3.48 | 17.05 | −0.35 | 26.36 | 15.43 | 21.48 | 0.52 | −8.68 | 15.43 |
| L2_11 | 54320.46 | 1.79 | 5.89 | 4.05 | 1400.5 | 1366.5 | 1395.3 | 1362.0 | 3.15 | 19.31 | −1.10 | 16.07 | 16.33 | 16.20 | −1.67 | −15.42 | 16.45 |
| L2_12 | 50831.15 | 1.01 | 7.03 | 4.12 | 1194.9 | 1165.5 | 1262.6 | 1236.9 | 3.12 | 17.92 | 0.25 | 15.75 | 16.16 | 20.13 | −0.41 | −14.63 | 17.86 |
| L2_13 | 84396.97 | 1.89 | 6.43 | −0.35 | 1648.2 | 1609.8 | 2148.9 | 2117.1 | 4.58 | 18.52 | 0.67 | 15.83 | 15.30 | 17.76 | 1.80 | −24.01 | 15.92 |
| L2_14 | 66753.89 | 2.38 | 6.37 | 0.02 | 1180.0 | 1156.2 | 1326.0 | 1287.2 | 2.15 | 19.36 | −2.44 | 16.86 | 15.87 | 15.32 | 0.19 | −20.64 | 16.08 |
| L2_15 | 81144.27 | 0.87 | 6.06 | 1.26 | 1625.3 | 1578.6 | 1910.5 | 1861.7 | 3.59 | 18.54 | 0.08 | 12.44 | 16.65 | 21.26 | −0.13 | −26.27 | 20.48 |
| L2_16 | 57747.57 | 1.70 | 6.71 | −3.20 | 1245.5 | 1216.0 | 1404.8 | 1360.9 | 4.69 | 12.90 | −0.21 | 18.31 | 14.13 | 18.44 | 0.06 | −12.77 | 16.31 |
| L2_17 | 43608.00 | 1.39 | 7.72 | 2.12 | 1101.0 | 1086.1 | 1241.4 | 1217.1 | 7.12 | 16.95 | 0.675 | 7.35 | 14.99 | 18.00 | 1.01 | −22.96 | 15.91 |
| L2_18 | 35746.32 | 1.65 | 6.22 | 0.30 | 869.2 | 851.9 | 1025.5 | 1000.1 | 4.86 | 17.94 | 0.35 | 12.73 | 15.27 | 16.73 | −0.57 | −21.40 | 15.17 |
| L2_19 | 76345.79 | 1.44 | 7.19 | −2.4 | 1471.3 | 1430.2 | 1798.7 | 1760.9 | 4.03 | 17.78 | 0.16 | 21.09 | 15.36 | 19.62 | 1.16 | −16.34 | 15.67 |
| L2_20 | 52575.81 | 1.4 | 6.46 | 4.08 | 1297.7 | 1266.0 | 1328.9 | 1299.4 | 3.13 | 18.61 | −0.42 | 15.91 | 16.24 | 18.16 | −1.04 | −15.02 | 17.15 |
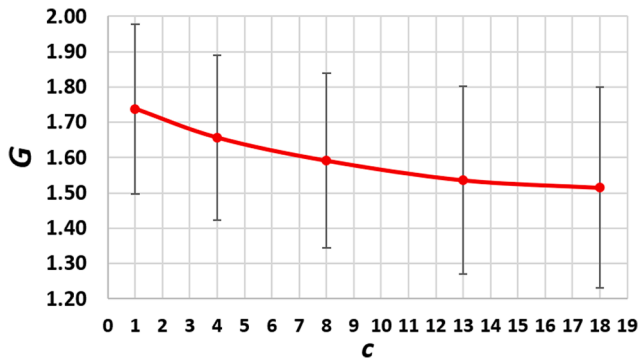
**Fig. 5.** Generalisation (G).
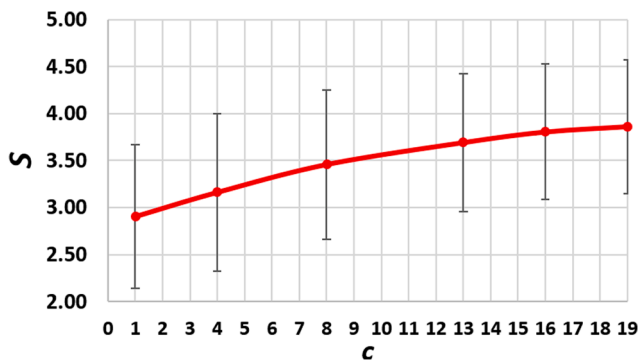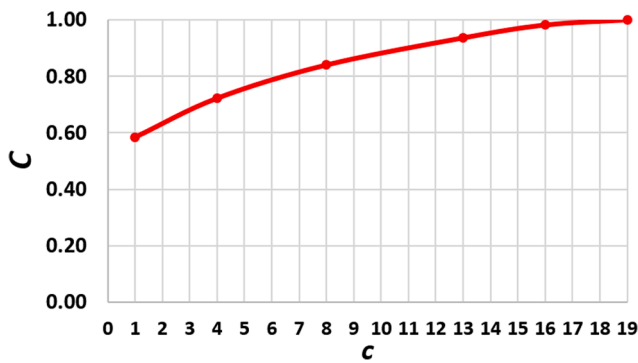


**Fig. 6.** Specificity (S).



**Fig. 7.** Compactness (C).

which decreases as $c$ (the number of MoVs) increases. This result is directly related to the low number of training samples. By enlarging the TS, G is expected to improve significantly, as shown by the slope of the G curve in Fig. 5: it is still far from being horizontal, even when considering all the MoVs.

In contrast to G, S does not offer quantitative information about the SSM itself (it is intended to compare different SSMs); it is valuable for qualitatively assessing the robustness of the SSM in reproducing coherent shapes. S is estimated by generating random parameters $\alpha$; for each $\alpha$, the SSM generates a new shape. The distance of each generated shape to the closest match of the TS is averaged over many runs (in this application, 100,000 runs). S is expected to increase as $c$ increases because, by increasing $c$, the SSM becomes more capable of deviating from the training shapes. However, this increment should be constrained, as the resulting models must remain coherent with the family of shapes represented by the training samples. Consequently, as $c$ increases, each added MoV has a diminishing effect on S, which must

result in the typical trend as illustrated in Fig. 6.

Finally, C represents the cumulative variance of the model as calculated with the PCA. In this application, the value of C is normalised with the total variance.

G, S, and C show the expected behaviour, confirming as much as possible the effectiveness of the performed SSA.

Once the SSM was obtained, the mean shape was segmented using the AFRM. As described above, a specific label (a number from 1 to 9, Table 2), positioned in the fourth column, was introduced as an encoder for the segmentation in the data matrix of the mean shape (Fig. 8).

### 4.2. eSSM application

The resulting eSSM can now fit a target shape and transfer the semantic segmentation to it, enabling the recognition and measurement of its dimensional features. In this paper, the performances of the eSSM was tested on the five L2 vertebrae that were not considered in the TS (Fig. 9a). First, the proposed eSSM was analysed qualitatively by comparing the obtained morphological segmentations with those provided by the AFRM (Fig. 9b). Then, each obtained morphological feature configuration was analysed to calculate the corresponding dimensional feature according to Di Angelo et al. [9]. The table in Fig. 9c depicts the percentage and absolute differences between the dimensional features provided by the eSSM, considering the results obtained with the AFRM as a reference. The Euclidean distance was determined to quantitatively analyse the difference in the position of the centre of the facet joints ($\mathbf{c}_{saf}$ and $\mathbf{c}_{iaf}$). Fig. 9b and 9c confirm that the eSSM provided similar results as the AFRM, which is assumed to be the ground truth in this application. The difference between the two methods is attributed to the eSSM's approximation of the anatomy, which is related to the fitting error discussed above.

While the results are comparable (and, in any case, still improvable for the new approach by increasing the number and quality of training cases), the significantly lower computational time makes the eSSM a highly efficient alternative to automatic segmentation methods. In particular, by using a laptop with a 2.80 GHz Intel i7 processor and 16.0 GB of RAM, the following elaboration times were registered:

- eSSM generation of a segmented vertebra ~ 10 s;
- AFRM segmentation process ~ 300 min.

The high processing time with the AFRM is primarily attributed to the skeletonisation algorithm, which necessitates computational optimisation. When evaluating the time required for the eSSM to generate a segmented vertebra, it is important to account for both the training process, which took about 10 min on the same laptop described above, and the segmentation of the mean shape. It is also worth noting that these operations only need to be completed once and not for each target vertebra.

In addition to its low computational time, a significant advantage of the eSSM is its ability to provide consistent results even with incomplete target models. It achieves this outcome by inferring the most likely shape of the complete model within the domain the TS allows. To assess this capability, the eSSM was used to obtain the semantic segmentation on four test cases with synthetic defects added (Fig. 10a):

- *Test#1A$_I$* and *Test#2A$_I$* were obtained by erasing, respectively, the whole left transverse process in *Test#1$_I$* and *Test#2$_I$*;
- *Test#1B$_I$* and *Test#2B$_I$* were obtained by erasing a large body area in *Test#1$_I$* and *Test#2$_I$*, respectively.

The four test cases belong to the five models used in the previous step and, consequently, were not included in the TS.

Fig. 10b shows the morphological feature recognition resulting from using the AFRM and the new approach with the AFRM and the eSSM. As
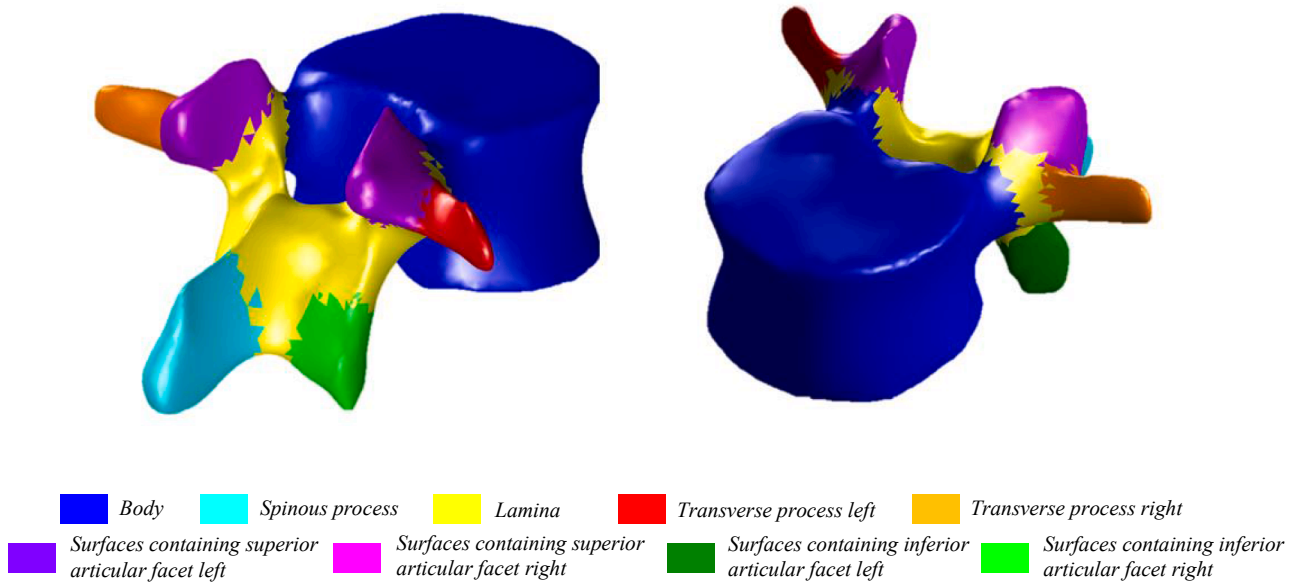
*Body*    *Spinous process*    *Lamina*    *Transverse process left*    *Transverse process right*

*Surfaces containing superior articular facet left*    *Surfaces containing superior articular facet right*    *Surfaces containing inferior articular facet left*    *Surfaces containing inferior articular facet right*

**Fig. 8.** Two views of the segmented mean shape for the two L2 vertebra.

already pointed out by Di Angelo et al. [9], the AFRM fails when a morphological feature is absent (as in *Test#1A$_I$* and *Test#1B$_I$*) or when its morphology is very different from the expected one (as in *Test#2A$_I$* and *Test#2B$_I$*). On the contrary, the results confirmed the robustness of the novel approach in morphological feature recognition when there are large missing areas.

It is worth noting that there are still issues to consider related to using an SSA-based method. Such issues are shown in Fig. 10c, which, as an example of the results, reports the following:

- On the left, the deviation map between the reconstructed target shapes (*Test#1A$_{eSSM}$* at the top and *Test#1B$_{eSSM}$* at the bottom of the figure) and the original non-defective model, *Test#1$_I$*;
- On the right, the deviation map between the reconstructed vertebrae *Test#1A$_{eSSM}$* and *Test#1B$_{eSSM}$* at the top and *Test#2A$_{eSSM}$* and *Test#2B$_{eSSM}$* at the bottom of the figure.

Both the deviation maps are provided as point-to-point distances, and the measures are in millimetres.

The deviation maps illustrate how the known data of the target shape influence the results of the fitting process. The maps on the left of Fig. 10c highlight that the fitting error is related to the extent of the missing information rather than the absence of a whole feature. On the right side, the maps show that starting from different *a priori* data, despite being derived from the same original shape, leads to different reconstructions. Both of these errors are typical in an SSA-based method, but they are expected to decrease by improving the variety of the TS.

## 5. Discussion

Analysing and measuring vertebrae are tasks conducted for various purposes, including to study anatomy, to diagnose disease, and to evaluate treatments. Due to the 3D distribution and complexity of morphological features, the quantitative recognition and assessment of a vertebra require a skilled operator, resulting in cumbersome and time-consuming procedures with inherently low repeatability and reproducibility. For these reasons, Di Angelo et al. [9] proposed the AFRM, which automatically performs semantic segmentation and dimensional characterisation of the thoracic and lumbar vertebrae. While the AFRM has demonstrated its robustness in providing a reliable outcome, it necessitates a discrete model of the vertebra defined as a high-density point

cloud with an input resolution of approximately 0.5 mm. In addition, it requires the presence of all morphological features, even if incomplete, and demands a high computational time because of the required complex analysis of geometric differential properties.

This paper has introduced an innovative upgrade to the AFRM based on the eSSM, which aims to incorporate more than just geometric information within the statistical framework. In this context, supplementary information is derived from semantic segmentation applied to the mean shape of the SSM by using the AFRM. The resulting eSSM can fit a target shape and transfer the semantic segmentation onto it. As stated in Section 3, the eSSM was chosen over predictive methods by considering the limitations imposed by the dataset's constraints (mainly related to the availability of training samples), the incoherence between the TS (healthy vertebrae) and potential targets (partially missed vertebrae), and the fact that the data have specific shape-based characteristics that align well with the strengths of SSA.

In this research, the eSSM was constructed for adult male healthy L2 vertebrae, employing 20 training samples. Once the training step was completed, tests were conducted involving five distinct L2 healthy vertebrae, which were not included in the TS. Furthermore, synthetic defects were introduced into two of the five models to evaluate the method's capability to provide consistent results despite large missing areas. The evaluation entailed comparing the segmentation of the test shapes produced by the novel approach and that generated by the AFRM, which, due to its established robustness and reliability, was employed as the ground truth to validate the segmentation. For the models with synthetic defects, the segmentation from the combination of the AFRM and the eSSM was also compared with the segmentation related to the healthy anatomy. The results showed the efficacy of the proposed technique, which brings together the strengths of the AFRM and the eSSM, guaranteeing robust and automated segmentation through the AFRM and capitalising on the eSSM's ability to produce consistent outcomes with a significantly reduced computational load, even when dealing with sparsely populated or partially incomplete target models.

The ability to operate with low-density point clouds enables the consideration of low-resolution CT or MRI scans as sources for generating the target model, thereby reducing patient exposure to radiation. The eSSM can still generate the most probable shape within the domain defined by the training samples, given the a-priori known data. Naturally, the greater the available *a priori* information, the more accurate
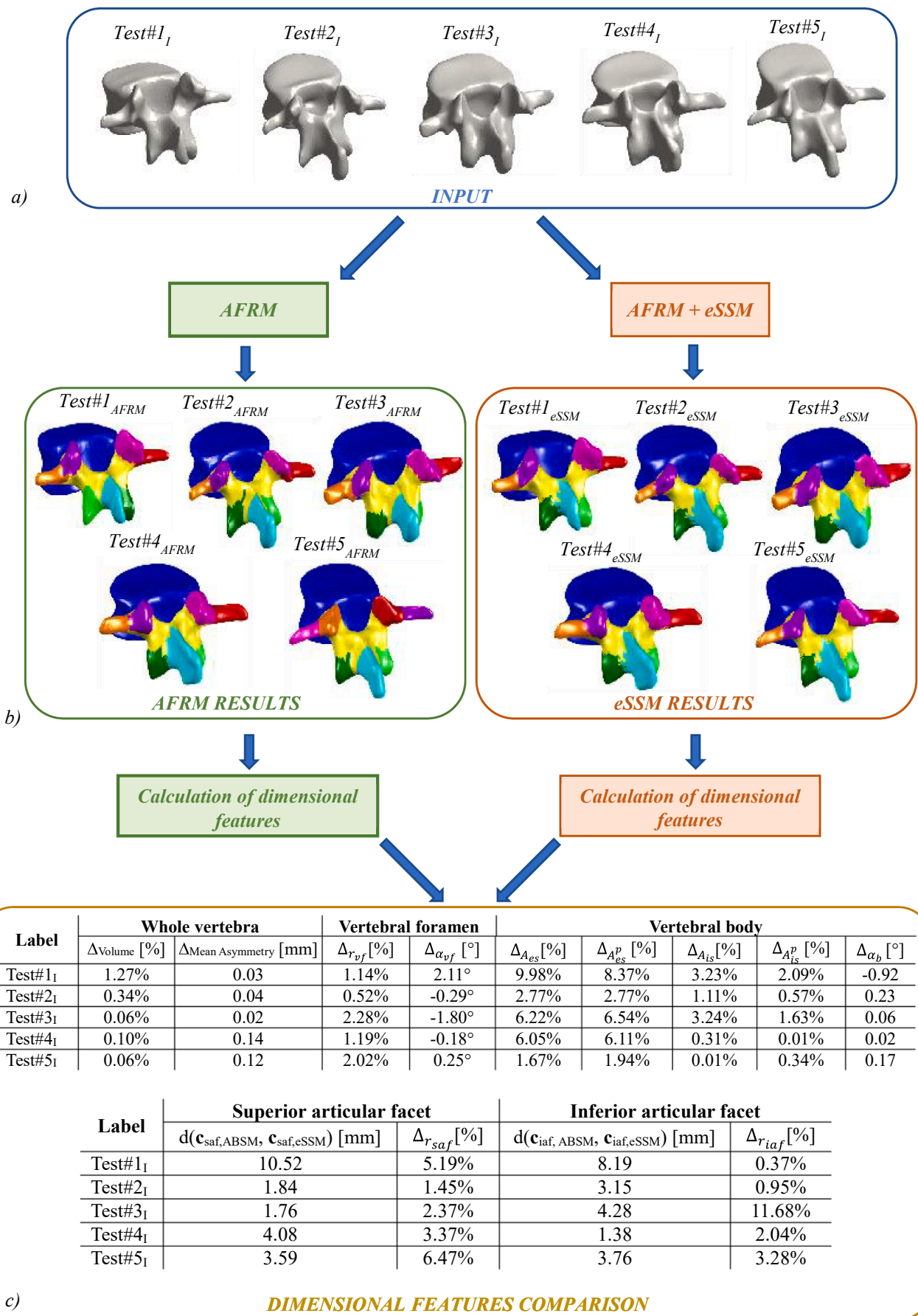
a) **INPUT**

Test#1$_I$  Test#2$_I$  Test#3$_I$  Test#4$_I$  Test#5$_I$

**AFRM**                    **AFRM + eSSM**

b)

Test#1$_{AFRM}$  Test#2$_{AFRM}$  Test#3$_{AFRM}$    Test#1$_{eSSM}$  Test#2$_{eSSM}$  Test#3$_{eSSM}$

Test#4$_{AFRM}$  Test#5$_{AFRM}$    Test#4$_{eSSM}$  Test#5$_{eSSM}$

**AFRM RESULTS**    **eSSM RESULTS**

*Calculation of dimensional features*    *Calculation of dimensional features*

| Label | Whole vertebra | | Vertebral foramen | | Vertebral body | | | | |
|---|---|---|---|---|---|---|---|---|---|
| | $\Delta$Volume [%] | $\Delta$Mean Asymmetry [mm] | $\Delta_{r_{vf}}$[%] | $\Delta_{\alpha_{vf}}$ [°] | $\Delta_{A_{es}}$[%] | $\Delta_{A_{es}^p}$ [%] | $\Delta_{A_{is}}$ [%] | $\Delta_{A_{is}^p}$ [%] | $\Delta_{\alpha_b}$ [°] |
| Test#1$_I$ | 1.27% | 0.03 | 1.14% | 2.11° | 9.98% | 8.37% | 3.23% | 2.09% | -0.92 |
| Test#2$_I$ | 0.34% | 0.04 | 0.52% | -0.29° | 2.77% | 2.77% | 1.11% | 0.57% | 0.23 |
| Test#3$_I$ | 0.06% | 0.02 | 2.28% | -1.80° | 6.22% | 6.54% | 3.24% | 1.63% | 0.06 |
| Test#4$_I$ | 0.10% | 0.14 | 1.19% | -0.18° | 6.05% | 6.11% | 0.31% | 0.01% | 0.02 |
| Test#5$_I$ | 0.06% | 0.12 | 2.02% | 0.25° | 1.67% | 1.94% | 0.01% | 0.34% | 0.17 |

| Label | Superior articular facet | | Inferior articular facet | |
|---|---|---|---|---|
| | d($\mathbf{c}_{saf,ABSM}$, $\mathbf{c}_{saf,eSSM}$) [mm] | $\Delta_{r_{saf}}$[%] | d($\mathbf{c}_{iaf, ABSM}$, $\mathbf{c}_{iaf,eSSM}$) [mm] | $\Delta_{r_{iaf}}$[%] |
| Test#1$_I$ | 10.52 | 5.19% | 8.19 | 0.37% |
| Test#2$_I$ | 1.84 | 1.45% | 3.15 | 0.95% |
| Test#3$_I$ | 1.76 | 2.37% | 4.28 | 11.68% |
| Test#4$_I$ | 4.08 | 3.37% | 1.38 | 2.04% |
| Test#5$_I$ | 3.59 | 6.47% | 3.76 | 3.28% |

c) **DIMENSIONAL FEATURES COMPARISON**

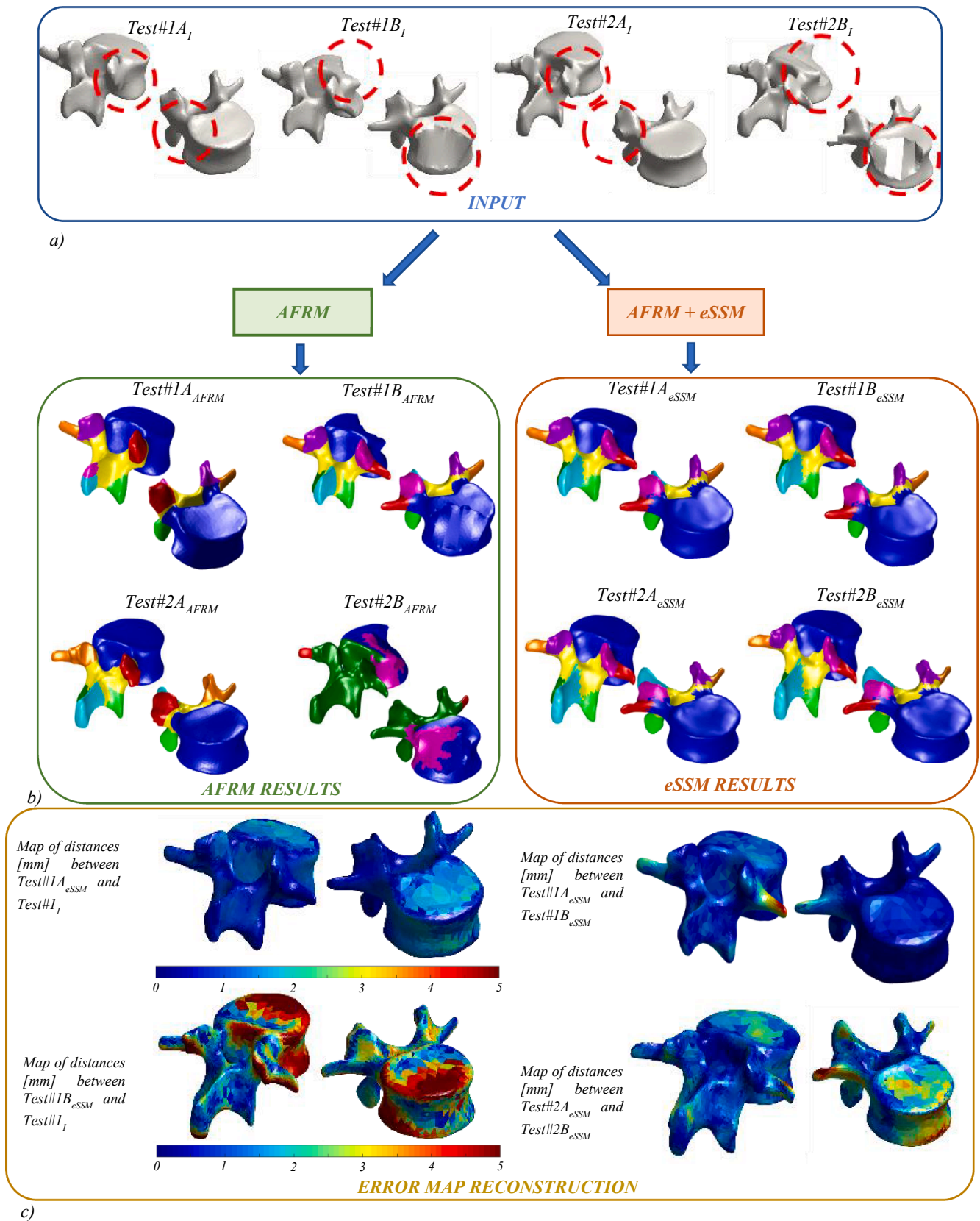**Fig. 9.** Test results of the robustness of the morphological feature recognition.

**Fig. 10.** Test results of the robustness of the morphological feature reconstruction of incomplete vertebrae.

the approximation provided by the eSSM.

A significant limitation to the research presented in this paper is the restricted availability of the initial data set. Given its nature as a population-based model, the accuracy of the eSSM is intrinsically tied to the quality of the training samples. This quality, in turn, relies not only on the quantity of training samples, but also on the inherent consistency of the data, aiming to represent the population as comprehensively as possible. The limited availability of training samples leads to an eSSM with a reduced ability to accurately represent the variability of the specific population being studied (in this application, the L2 vertebra for an adult). Future efforts must be made to improve the quality of the TS.

## 6. Conclusion

The proposed method combines the benefits of the AFRM and eSSM approaches. It ensures reliable and automated segmentation via the AFRM while leveraging the eSSM's ability to provide results even when dealing with sparsely populated or partially incomplete target models, consistently reducing the computational load. The main limitation of the proposed method is the need for a consistent TS representing the population as comprehensively as possible. An inconsistent or incomplete TS reduces the eSSM's capability to accurately represent the variability of the population being investigated. Future efforts will aim to assemble more extensive databases to construct a complete parametric and generative atlas of human vertebrae with additional semantic segmentation information.

In conclusion, the main objective of this paper was to assess the eSSM's potential in conjunction with the AFRM, aiming to produce reliable and robust results while mitigating the limitations of the latter method. Within the scope of this evaluation and recognising the inherent limitations, the obtained results validate the applicability of the proposed approach.

## CRediT authorship contribution statement

**Antonio Marzola:** Writing – review & editing, Writing – original draft, Software, Methodology, Investigation, Formal analysis, Data curation, Conceptualization. **Luca Di Angelo:** Writing – review & editing, Writing – original draft, Visualization, Software, Project administration, Methodology, Investigation, Formal analysis, Data curation, Conceptualization. **Paolo Di Stefano:** Writing – review & editing, Validation, Supervision, Resources, Project administration, Methodology. **Yary Volpe:** Writing – review & editing, Validation, Supervision, Resources, Project administration, Conceptualization.

## Declaration of competing interest

The authors declare that they have no known competing financial interests or personal relationships that could have appeared to influence the work reported in this paper.

## Data availability

The data that has been used is confidential.

## Appendix A. Supplementary material

Supplementary data to this article can be found online at https://doi.org/10.1016/j.bspc.2024.105972.

## References

[1] J.-P. Steib, R. Dumas, D. Mitton, W. Skalli, Surgical correction of scoliosis by in situ contouring, Spine 29 (2004) 193–199, https://doi.org/10.1097/01.BRS.0000107233.99835.A4.

[2] M.-L. Nault, J.-M. Mac-Thiong, M. Roy-Beaudry, I. Turgeon, J. deGuise, H. Labelle, S. Parent, Three-dimensional spinal morphology can differentiate between progressive and nonprogressive patients with adolescent idiopathic scoliosis at the initial presentation, Spine 39 (2014) E601–E606, https://doi.org/10.1097/BRS.0000000000000284.

[3] E. Ferrero, R. Lafage, B.G. Diebo, V. Challier, B. Illharreborde, F. Schwab, W. Skalli, P. Guigui, V. Lafage, Tridimensional analysis of rotatory subluxation and sagittal spinopelvic alignment in the setting of adult spinal deformity, Spine Deform. 5 (2017) 255–264, https://doi.org/10.1016/j.jspd.2017.01.003.

[4] H.-D. Wu, M.-S. Wong, Assessment of maximum spinal deformity in scoliosis: a literature review, J. Med. Biol. Eng. 40 (2020) 621–629, https://doi.org/10.1007/s40846-020-00558-z.

[5] Y. Wang, M.C. Battié, T. Videman, A morphological study of lumbar vertebral endplates: radiographic, visual and digital measurements, Eur. Spine J. 21 (2012) 2316–2323, https://doi.org/10.1007/s00586-012-2415-8.

[6] M. Kishimoto, K. Akeda, A. Sudo, A.A. Espinoza Orías, N. Inoue, In vivo measurement of vertebral endplate surface area along the whole-spine, J. Orthop. Res. 34 (2016) 1418–1430, https://doi.org/10.1002/jor.23354.

[7] Y. Otsuka, H.S. An, R.S. Ochia, G.B.J. Andersson, A.A. Espinoza Orías, N. Inoue, In vivo measurement of lumbar facet joint area in asymptomatic and chronic low back pain subjects, Spine 35 (2010) 924–928, https://doi.org/10.1097/BRS.0b013e3181c9fc04.

[8] P. Simon, A.A. Espinoza Orías, G.B.J. Andersson, H.S. An, N. Inoue, In vivo topographic analysis of lumbar facet joint space width distribution in healthy and symptomatic subjects, Spine 37 (2012) 1058–1064, https://doi.org/10.1097/BRS.0b013e3182552ec9.

[9] L. Di Angelo, P. Di Stefano, E. Guardiani, An automatic method for feature segmentation of human thoracic and lumbar vertebrae, Comput. Methods Programs Biomed. 210 (2021) 106360, https://doi.org/10.1016/j.cmpb.2021.106360.

[10] R. Jakubicek, J. Chmelik, J. Jan, P. Ourednicek, L. Lambert, G. Gavelli, Learning–based vertebra localization and abelling in 3D CT data of possibly incomplete and pathological spines, Comput. Methods Programs Biomed. 183 (2020) 105081, https://doi.org/10.1016/j.cmpb.2019.105081.

[11] S. Guinebert, E. Petit, V. Bousson, S. Bodard, N. Amoretti, B. Kastler, Automatic semantic segmentation and detection of vertebras and intervertebral discs by neural networks, Comp. Methods Programs Biomed. Update 2 (2022) 100055, https://doi.org/10.1016/j.cmpbup.2022.100055.

[12] S. Banerjee, J. Lyu, Z. Huang, H.F.F. Leung, T.-T.-Y. Lee, D. Yang, S. Su, Y. Zheng, S.-H. Ling, Light-convolution dense selection U-net (LDS U-Net) for ultrasound lateral bony feature segmentation, Appl. Sci. 11 (2021) 10180, https://doi.org/10.3390/app112110180.

[13] M. Rak, J. Steffen, A. Meyer, C. Hansen, K. Tönnies, Combining convolutional neural networks and star convex cuts for fast whole spine vertebra segmentation in MRI, Comput. Methods Programs Biomed. 177 (2019) 47–56, https://doi.org/10.1016/j.cmpb.2019.05.003.

[14] R.F. Masood, I.A. Taj, M.B. Khan, M.A. Qureshi, T. Hassan, Deep learning based vertebral body segmentation with extraction of spinal measurements and disorder disease classification, Biomed. Signal Process. Control. 71 (2022) 103230, https://doi.org/10.1016/j.bspc.2021.103230.

[15] P. Cheng, X. Cao, Y. Yang, G. Zhang, Y. He, Automatically recognize and segment morphological features of the 3D vertebra based on topological data analysis, Comput. Biol. Med. 149 (2022) 106031, https://doi.org/10.1016/j.compbiomed.2022.106031.

[16] H. Carr, J. Tierny, G.H. Weber, Pathological and Test Cases for Reeb Analysis, in: H. Carr, I. Fujishiro, F. Sadlo, S. Takahashi (Eds.), Topological Methods in Data Analysis and Visualization V, Springer, Cham, 2020, pp. 103–120. Doi: 10.1007/978-3-030-43036-8_7.

[17] T. Klinder, J. Ostermann, M. Ehm, A. Franz, R. Kneser, C. Lorenz, Automated model-based vertebra detection, identification, and segmentation in CT images, Med. Image Anal. 13 (2009) 471–482, https://doi.org/10.1016/j.media.2009.02.004.

[18] F. Reinders, M.E.D. Jacobson, F.H. Post, Skeleton graph generation for feature shape description, in: W.C. de Leeuw, R. Liere (Eds.), Data Visualization 200. Eurographics, Springer, Vienna, 2000, pp. 73–82. Doi: 10.1007/978-3-7091-6783-0_8.

[19] F. Ambellan, H. Lamecker, C. von Tycowicz, S. Zachow, Statistical shape models: understanding and mastering variation in anatomy, in: P. Rea (Ed.), Biomedical Visualisation, Springer, Cham, 2019, pp. 67–84. Doi: 10.1007/978-3-030-19385-0_5.

[20] T. Heimann, H.-P. Meinzer, Statistical shape models for 3D medical image segmentation: a review, Med. Image Anal. 13 (2009) 543–563, https://doi.org/10.1016/j.media.2009.05.004.

[21] A. Marzola, K.S. McGreevy, F. Mussa, Y. Volpe, L. Governi, HyM3D: a hybrid method for the automatic 3D reconstruction of a defective cranial vault, Comput. Methods Programs Biomed. 234 (2023) 107516, https://doi.org/10.1016/j.cmpb.2023.107516.

[22] A. Marzola, F. Buonamici, L. Guariento, L. Governi, Enhanced statistical shape model: a statistical-based tool to design custom orthopaedic devices, in: C. Rizzi, F. Campana, M. Bici, F. Gherardini, T. Ingrassia, P. Cicconi (Eds.), Design Tools and Methods in Industrial Engineering II. ADM 2021. Lecture Notes in Mechanical Engineering, Springer, Cham, 2022, pp. 27–38. Doi: 10.1007/978-3-030-91234-5_3.

[23] A. Sances, J.B. Myklebust, D.J. Maiman, S.J. Larson, J.F. Cusick, R.W. Jodat, The biomechanics of spinal injuries, Crit. Rev. Biomed. Eng. 11 (1984) 1–76.

[24] D. Woodhouse, Post-traumatic compression fracture, Clin. Chiropr. 6 (2003) 67–72, https://doi.org/10.1016/S1479-2354(03)00020-8.

[25] M. El-Rich, P.-J. Arnoux, E. Wagnac, C. Brunet, C.-E. Aubin, Finite element investigation of the loading rate effect on the spinal load-sharing changes under impact conditions, J. Biomech. 42 (2009) 1252–1262, https://doi.org/10.1016/j.jbiomech.2009.03.036.

[26] R.H. Davies, Learning shape: optimal models for analyzing natural variability, University of Manchester, 2004.